Frontiers in Bioscience Landmark

Front. Biosci. (Landmark Ed) **2025**; 30(9): 45020
https://doi.org/10.31083/FBL45020

Original Research

PTDSS1 Drives Glycolysis and Malignant Progression of Lung Cancer Through Maintaining Nuclear–Mitochondrial Homeostatic Crosstalk

Hailun Wang[1], Qiao Wang[2], Yandu He[1], Xuelu Pu[1], Yajun Li[3,*]

[1]Department of Oncology, The Third Affiliated Hospital of Zunyi Medical University (The First People's Hospital of Zunyi), 563099 Zunyi, Guizhou, China
[2]Department of Medical Oncology, Guizhou Province People's Hospital, 550002 Guiyang, Guizhou, China
[3]Department of Oncology, The Eighth Affiliated Hospital, Southern Medical University (The First People's Hospital of Shunde Foshan), 528399 Foshan, Guangdong, China
*Correspondence: yajun790@zmu.edu.cn (Yajun Li)
Academic Editor: Jordi Sastre-Serra
Submitted: 16 July 2025 Revised: 25 August 2025 Accepted: 12 September 2025 Published: 26 September 2025

Abstract

Background: Phosphatidylserine synthase 1 (PTDSS1) is a crucial enzyme involved in phospholipid synthesis. However, its role in the metabolic regulation of lung cancer remains unclear. This study hypothesized that PTDSS1 promotes lung cancer progression by regulating metabolic reprogramming through nuclear–mitochondrial crosstalk. **Methods**: PTDSS1's expression levels in lung cancer tissues and their correlation with patient prognosis were evaluated through bioinformatics analysis and immunohistochemistry. *In vitro* functional experiments, including cell proliferation, migration, invasion, and colony formation, were performed using PTDSS1-overexpressing lung cancer cell lines. Cellular glycolysis and mitochondrial oxidative phosphorylation levels were determined. PTDSS1's subcellular localization was investigated through cellular fractionation and immunofluorescence. Its regulatory interaction with pyruvate kinase M2 (*PKM2*) was examined. Expression levels of metabolism-related genes and mitochondrial dynamics markers were analyzed by qRT-PCR and Western blot. **Results**: PTDSS1 was significantly overexpressed in lung cancer tissues. High PTDSS1 expression correlated with poor patient prognosis. PTDSS1 enhanced lung cancer cell proliferation, migration, and invasion capabilities. Metabolically, PTDSS1 promoted aerobic glycolysis. Mitochondrial oxidative phosphorylation was suppressed. Nuclear-localized PTDSS1 showed enhanced effectiveness in driving glycolysis and malignant progression. Mechanistically, PTDSS1 may accelerate glycolysis through *PKM2* regulation. It may drive lung cancer progression through PKM2-mediated nuclear–mitochondrial homeostatic crosstalk. **Conclusion**: PTDSS1 functions as a multifunctional oncogene. It drives lung cancer progression through PKM2-mediated nuclear–mitochondrial homeostatic crosstalk. PTDSS1 represents a potential prognostic biomarker and therapeutic target.

Keywords: lung cancer; PTDSS1; glycolysis; nuclear-mitochondrial crosstalk; PKM2

1. Introduction

Metabolic reprogramming in tumor cells is recognized as one of the hallmark features during cancer development and progression [1,2]. The most characteristic phenomenon is the Warburg effect, whereby tumor cells preferentially obtain energy through glycolysis even under oxygen-sufficient conditions [3,4]. This metabolic shift provides energy and biosynthetic precursors for tumor cell growth, proliferation, invasion, and metastasis, but the precise regulatory mechanisms remain incompletely elucidated [5]. In particular, the role of nuclear-mitochondrial communication and coordination in regulating tumor metabolism and promoting tumor progression continues to be a challenging focal point in cancer research [6,7].

Phosphatidylserine synthase 1 (PTDSS1) is a critical enzyme located on the endoplasmic reticulum membrane that primarily catalyzes the synthesis of phosphatidylserine (PS), an essential component of cell membranes that plays significant roles in maintaining membrane integrity and cellular signal transduction [8,9]. Phospholipid metabolism is closely associated with tumorigenesis and progression [8,10]. Given the importance of lipid metabolism in cancer development, the present study investigated whether PTDSS1 plays a role in lung cancer progression. Limited studies have indicated that PTDSS1 expression is upregulated in certain tumor types, but its expression pattern and functional significance in lung cancer remain unclear. Recent research has shown that PTDSS1 expression levels correlate with tumor progression in some cancer types [10]. High PTDSS1 expression is associated with tumor invasion and poor prognosis. Additionally, studies suggest that PTDSS1 may participate in tumor progression by influencing lipid metabolism [10,11]. Recent evidence suggests that enzymes involved in lipid metabolism, including PTDSS1, may have broader roles in cancer beyond their classical functions. However, the specific contribution of PTDSS1 to lung cancer remains largely unexplored.

Cellular metabolic reprogramming, particularly enhanced glycolysis, is a critical characteristic of tumor progression [12–14]. The relationship of PTDSS1 with

key glycolytic enzymes was examined to understand the metabolic mechanisms underlying its potential oncogenic role. Pyruvate kinase M2 (*PKM2*), as one of the rate-limiting enzymes in glycolysis, plays a pivotal role in tumor metabolism [15,16]. Unlike other pyruvate kinase isoforms, PKM2 is highly expressed in tumor cells and possesses unique regulatory properties, not only participating in glycolytic reactions in the cytoplasm but also translocating to the nucleus to function as a transcriptional co-activator, thus influencing the expression levels of various metabolism-related genes [17,18]. However, how PKM2 expression and activity are regulated, especially the precise regulatory mechanisms during lung cancer development, remains incompletely understood.

Metabolic reprogramming in cancer involves glycolytic enhancement and mitochondrial adaptation. The mitochondria are central to cellular energy metabolism, and they serve as important regulatory organelles for apoptosis [19]. Recent studies have revealed that the balance of mitochondrial dynamics is crucial for maintaining cellular energy supply and apoptotic regulation [20,21]. Mitofusin 1/2 (*MFN1/2*) and peroxisome proliferator-activated receptor γ coactivator 1α (*PGC-1*α) are key factors regulating mitochondrial function and biogenesis. Research has shown that in certain tumors, mitochondrial dysfunction is closely linked to metabolic reprogramming and apoptosis resistance in tumor cells [22]. However, the relationship between mitochondrial homeostasis and lung cancer progression, particularly the synergistic pattern with cellular metabolic alterations, requires further investigation. Nuclear-mitochondrial crosstalk is a complex bidirectional regulatory process essential for maintaining cellular homeostasis [23,24]. Evidence suggests that dysregulation of this communication mechanism contributes to various diseases, including cancer [25]. However, current research on the role of nuclear-mitochondrial communication in lung cancer progression, especially its association with metabolic reprogramming, remains relatively limited. Although studies have indicated that certain transcription factors and signaling molecules are involved in regulating this process, the overall regulatory network of nuclear-mitochondrial synergy, particularly the identification and functional validation of key regulatory molecules, remains an important direction in current research.

On the basis of the evidence linking PTDSS1 to lipid metabolism and the critical role of metabolic reprogramming in cancer, PTDSS1 is hypothesized to be driving lung cancer progression by coordinating nuclear-mitochondrial communication to regulate glycolytic metabolism. Specifically, this study proposes that PTDSS1 promotes glycolysis through PKM2-mediated pathways while maintaining mitochondrial homeostasis to support tumor cell survival and metastasis.

2. Materials and Methods

2.1 TCGA Data Analysis

This study utilized publicly available transcriptomic data from The Cancer Genome Atlas (TCGA) database. Transcriptome data of patients with lung adenocarcinoma were obtained from TCGA database to analyze *PTDSS1* expression differences between tumor tissues and adjacent normal tissues, its correlation with clinicopathological features, and its relationship with patient survival. Data preprocessing included the following: (1) removal of samples with missing clinical information, (2) $\log_2$ transformation of expression values, and (3) filtering of genes with low expression (FPKM <1 in $>50\%$ samples). Survival curves were generated with the Kaplan-Meier method, and group differences were assessed using the log-rank test.

2.2 LinkedOmics Database Analysis

The LinkedOmics database (http://www.linkedomics.org) provides multi-omics and clinical data for 32 cancer types and 11,158 TCGA patients. It features tools for analyzing multi-omics data and was used to study PTDSS1-associated co-expressed genes in lung cancer. The screening steps in this database were as follows: (1) select cancer cohort: Lung Adenocarcinoma (LUAD); (2) select search dataset: Data, stype: RNAseq; (3) select sample dataset: No input; and (4) select search dataset attribute: PTDSS1. Hierarchical clustering analysis of PTDSS1 co-expressed genes was performed using the LinkFinder module, with genes clustered on the basis of Pearson's correlation coefficients and visualized as heatmaps with dendrograms. Differential expression analysis and volcano plots were generated using the LinkCompare module, with significance determined by Pearson's correlation ($|\text{coefficient}| > 0.3$ and $p < 0.01$). The volcano plots displayed the correlation coefficients versus -log10 (p-value) to visualize positively and negatively correlated genes. Gene Ontology (GO) and Kyoto Encyclopedia of Genes and Genomes (KEGG) pathway enrichment analyses of PTDSS1 co-expressed genes were performed using the LinkInterpreter module through the clusterProfiler R package, with enrichment significance determined using hypergeometric test (False Discovery Rate (FDR) <0.05).

2.3 Cell Culture

Human lung adenocarcinoma cell lines A549 and NCI-H1299 were purchased from the American Type Culture Collection. All cell lines were validated by Short Tandem Repeat (STR) profiling and tested negative for mycoplasma. The cells were cultured in complete medium consisting of 90% high-glucose Dulbecco's Modified Eagle Medium (DMEM) (PM150210B; PronoCell, Heidelberg, Germany), 10% fetal bovine serum (Gibco, 10091148, Thermo Fisher Scientific, Waltham, MA, USA), and 1% penicillin–streptomycin (PB180120, PronoCell, Heidelberg, Germany) at 37 °C with 5% CO_2 and passaged as re-

quired. When the cell density in the six-well plates reached 70%–80%, the cells were transfected with OE-PTDSS1 (OE: Overexpression) plasmid and Short hairpin RNA (shRNA) (shPKM2, 5′-GTTCGGAGGTTTGATGAAATC-3′) plasmid (GenePharma, Shanghai, China) by using Lipofectamine 3000 (Thermo Fisher Scientific, L3000015, Thermo Fisher Scientific, Waltham, MA, USA). For each well, 2.5 µg of plasmid DNA was mixed with 5 µL of Lipofectamine 3000 reagent in 125 µL of Optimized Minimal Essential Medium (Opti-MEM), incubated for 15 min at room temperature, and then added dropwise to the cells in fresh medium without antibiotics. The plasmids used were as follows: pCDH-CMV-MCS-EF1-PTDSS1-Puro: full-length PTDSS1 overexpression plasmid and pCDH-CMV-MCS-EF1-NLS-PTDSS1-Puro: PTDSS1 overexpression plasmid containing nuclear localization signal peptide. OE-NC (overexpression negative control) cells were generated via transfection with empty pcDNA3.1 vector, and they served as controls for PTDSS1 overexpression experiments. pLKO.1-shPKM2: RNA interference plasmid targeting PKM2 transfection was performed using Lipofectamine 3000 reagent in accordance with the manufacturer's recommended protocol. Stable expression cell lines were obtained after 2 weeks of selection with 2 µg/mL of puromycin. Cisplatin (10 µM, 24 h, Sigma-Aldrich, C2211000, St. Louis, MO, USA) was used to induce cell apoptosis. 2-Deoxy-D-glucose (2-DG, 5 mM, 24 h, Sigma-Aldrich, D8375, St. Louis, MO, USA) was used as a glycolysis inhibitor. DMSO served as the control treatment group.

2.4 Western Blot Analysis

Total protein was extracted using Radioimmunoprecipitation Assay (RIPA) lysis buffer (P0013B, Beyotime Biotechnology, Shanghai, China). After cellular debris was removed, protein concentration was determined using BCA assay (P0012, Beyotime Biotechnology, Shanghai, China) with bovine serum albumin (BSA) standards ranging from 0 µg/mL to 2000 µg/mL. Proteins were denatured at 100 °C for 10 min, mixed with 4× laoding buffer, and heated at 95 °C for 10 min. The proteins (30 µg) were separated by electrophoresis using 12% SDS-PAGE (A3574, Sigma-Aldrich, St. Louis, MO, USA) and electrophoresed at 80 (stacking gel) and 120 V (resolving gel). The proteins were transferred to Polyvinylidene Fluoride (PVDF) membranes (0.45 µm, IPVH00010, Millipore, Billerica, MA, USA) via a wet transfer system at 100 V for 90 min at 4 °C (transfer buffer: 192 mM glycine, 25 mM Tris, and 20% methanol). After being blocked with 5% non-fat milk at 37 °C for 2 h, the membranes were incubated with PTDSS1 antibody (ab157222, Abcam, Cambridge, UK, 1:1000 dilution) overnight at 4 °C, followed by washing with Tris-Buffered Saline with Tween-20 (TBST) three times for 10 min each. Beta-actin (ab8226, Abcam, Cambridge, UK, 1:1000 dilution) was used as a loading control. Membranes were incubated with HRP-conjugated goat anti-rabbit IgG secondary antibody (ab6721, Abcam, 1:5000) at room temperature for 2 h, followed by three 10-min washes with TBST. Signals were captured using enhanced chemiluminescence (P0018FS, Beyotime Biotechnology, Shanghai, China).

2.5 qRT-PCR

RNA was extracted and converted to cDNA using a reverse transcription kit (15596026, Invitrogen, Carlsbad, CA, USA; reaction conditions: 37 °C for 45 min and 85 °C for 5 min; stored at 4 °C). RNA purity was assessed by measuring the A260/A280 ratios ($\geq$1.8 required) with a NanoDrop spectrophotometer (NanoDrop 2000; Thermo Fisher Scientific, Waltham, MA, USA). The β-actin gene was used as an internal reference, and RT-qPCR was employed to detect target gene expression levels. Primers were synthesized by Shanghai Sangon Biotech (Shanghai, China). An RNA reverse transcription kit (RR037A, TaKaRa Bio, Dalian, China) and a RT-qPCR detection kit (RR420A, TaKaRa Bio) were used. qPCR was conducted on a StepOne Plus system (Applied Biosystems, Thermo Fisher Scientific, Foster City, CA, USA) using SYBR Premix Ex Taq II (RR420A, TaKaRa Bio, Dalian, China) under the following conditions: 30 s at 95 °C, followed by 40 cycles of 5 s at 95 °C and 34 s at 60 °C. The sequences are shown in Table 1. Each sample was run in triplicate, and the average value was calculated. Determined using the $2^{-\Delta\Delta Ct}$ method.

2.6 Cell Viability Assay

Logarithmic phase cells were collected after trypsin digestion and centrifuged at 1000 r/min for 5 min. The supernatant was discarded, and cells were resuspended in fresh complete medium, adjusting the density to 5×10^4 cells/mL. A total of 100 µL was seeded in 96-well plates with 4 sets of 6 wells per group. For Cell Counting Kit-8 (CCK-8) detection, 10 µL of CCK-8 solution (CK04, Dojindo, Kumamoto, Japan) was added to six wells per group at each time point. Absorbance was measured at 450 and 620 nm after 3 h using a microplate reader.

2.7 EdU Cell Proliferation Assay

Cell proliferation was measured using the Click-iT 5-ethyl-2'-deoxyuridine (EdU) kit (C10340, Thermo Fisher Scientific Inc., Waltham, MA, USA). Cells were seeded in confocal plates (5×10^5 cells/well) and incubated with 50 µM EdU for 2 h at 37 °C. After fixing with 4% formaldehyde for 30 min and permeabilizing with 0.1% Triton X-100 for 20 min, cells were treated with Click-iT mixture. Nuclei were counterstained with 4',6-diamidino-2-phenylindole (DAPI) (D3571, Thermo Fisher Scientific, Waltham, MA, USA) and observed under a fluorescence microscope (Eclipse Ti-U; Nikon, Tokyo, Japan).

Table 1. Primer information.

Gene	Forward Primer (5′-3′)	Reverse Primer (5′-3′)
PKM2	ATGTCGAAGCCCCATAGTGAA	TGGGTGGTGAATCAATGTCCA
MFN1	TGACTCCAGCCATGTCCATCT	ACAGTCGAGCAAAAGTAGCCA
MFN2	CTCTCGATGCAACTCTATCGTC	TCCTGTACGTGTCTTCAAGGAA
PGC-1α	TTCCACCAAGAGCAAGTATGACTC	GCCTGAGCTTGTCCTTTGTTC
β-actin	CATGTACGTTGCTATCCAGGC	CTCCTTAATGTCACGCACGAT

PKM2, pyruvate kinase M2; *MFN1*, Mitofusin 1; *MFN2*, Mitofusin 2; *PGC-1α*, proliferator-activated receptor γ coactivator 1α.

2.8 Colony Formation Assay

Cells were seeded on glass coverslips at 1000 cells/well. After 7 days, the medium was removed, and cells were washed with Phosphate-Buffered Saline (PBS) and fixed with methanol for 20 min. Membranes were stained with a membrane dye for 30 min, and nuclei were counterstained with DAPI. Images were captured using an Olympus fluorescence microscope, and colonies were counted.

2.9 Transwell Invasion Assay

Each Matrigel-coated invasion chamber (BD Biosciences, #354234, Franklin Lakes, NJ, USA) was hydrated with 50 µL of serum-free medium for 30 min before aspirating the remaining medium. Cells were diluted in serum-free medium to 5×10^5 cells/mL, and 200 µL of this suspension (1000 cells) was added to the upper chamber, while the lower chamber received 500 µL of medium with 10% FBS. After 24 h of incubation, the upper chamber's medium was aspirated, and cells on the upper membrane surface were gently removed with cotton swabs. Cells were fixed with methanol for 20 min, washed thrice with PBS, and stained with crystal violet (Sigma-Aldrich, C6158, St. Louis, MO, USA) for 10 min. After three washes with water, cells were counted, photographed, and the results were represented as bar graphs showing the relative number of invaded cells.

2.10 Glucose Uptake and Lactate Secretion Measurement

Glucose uptake was measured using the fluorescent glucose analog 2-NBDG (N13195, Thermo Fisher Scientific, Waltham, MA, USA). After 2 h of serum starvation, cells were incubated with 2-NBDG (100 µM) for 30 min and washed with PBS. Then, fluorescence intensity was detected. Lactate secretion was determined using a lactate detection kit. Cell culture supernatants were collected and processed in accordance with the kit's instructions (MAK064, Sigma-Aldrich, St. Louis, MO, USA), and absorbance was measured at 570 nm by using a microplate reader (BioTek Instruments, Winooski, VT, USA).

2.11 Cellular Energy Metabolism Analysis

Oxygen consumption rate (OCR) and extracellular acidification rate (ECAR) were measured using a Seahorse XF96 analyzer (Agilent Technologies, Santa Clara, CA, USA). Cells were processed according to the Seahorse XF Cell Mito Stress Test (Agilent Technologies, 103020-100, Santa Clara, CA, USA) and Glycolysis Stress Test protocols after being seeded at a density of 1×10^4 cells per well in XF96 plates.

2.12 Immunofluorescence Staining

Cell coverslips were placed at the bottom of 24-well cell culture plates, and 1 mL of culture medium was added. The cells were seeded onto the coverslips at a density of 5×10^5 cells per well and cultured for 48 h at 37 °C with approximately 95% humidity and 5% CO_2. Coverslips were removed, then washed with cold PBS and fixed with 4% paraformaldehyde. After rinsing with running water, slides were incubated with goat serum at 37 °C for 20 min before discarding the serum., and primary antibodies with rabbit anti-PTDSS1 antibody (ab157222, Abcam, Cambridge, UK, 1:200) and PKM2 (BF8191, Affinity, Cincinnati, OH, USA, 1:200) were applied and incubated overnight at 4 °C. Approximately 50 µL of the corresponding secondary antibodies were applied to fully cover each section, followed by incubation at 37 °C for 20 min. Each coverslip was mounted with approximately 50 µL of anti-quenching mounting medium (containing DAPI), and images were captured using a laser confocal microscope (Nikon, Tokyo, Japan).

2.13 Cytoskeletal Staining

After removal, cell coverslips were fixed with 4% formaldehyde solution and subsequently permeabilized with 0.5% Triton X-100 solution (A16046.AE, Thermo Fisher Scientific, Waltham, MA, USA). The cells were then immunofluorescently stained with rhodamine-labeled phalloidin (C2207S, Beyotime Biotechnology, Shanghai, China) to visualize the cytoskeleton. Finally, the cytoskeletal structures were observed, and the cell lengths were quantified using confocal microscopy (Nikon, Japan).

2.14 Mitochondrial Staining and PTDSS1-Mitochondrion Co-localization Analysis

A549 and NCI-H1299 cells were cultured on coverslips and labeled with 100 nM MitoTracker Red CMXRos (M7512, Thermo Fisher Scientific, Waltham, MA, USA) at 37 °C for 30 min. Fixed with 4% paraformaldehyde, per-

meabilized with 0.2% Triton X-100 for 10 min, and blocked with 5% BSA for 1 h. They were then incubated overnight at 4 °C with rabbit anti-PTDSS1 antibody (ab157222, Abcam, Cambridge, UK, 1:200). Treated with Alexa Fluor 488-labeled secondary antibody (Thermo Fisher Scientific, A-11008, Waltham, MA, USA, 1:500) for 1 h at room temperature in the dark. Nuclei were stained with DAPI for 5 min before mounting. Three-channel fluorescence images (DAPI, PTDSS1-green, and mitochondria-red) were acquired.

2.15 TUNEL Apoptosis Detection

A549 and NCI-H1299 cells were seeded at a density of 5×10^4 cells/well in 24-well plates containing sterile coverslips and cultured overnight. All groups were treated with 10 μM cisplatin for 24 h to induce apoptosis. Cells were fixed with 4% paraformaldehyde, permeabilized with 0.2% Triton X-100. Subsequent procedures were performed in accordance with the Terminal deoxynucleotidyl transferase dUTP nick end labeling (TUNEL) apoptosis detection kit's instructions (11684817910, Roche, Basel, Switzerland) as follows: Cells were incubated with TUNEL reaction mixture (containing terminal deoxynucleotidyl transferase and fluorescent dUTP) for 1 h at 37 °C in the dark. After three PBS washes, they were mounted with DAPI-containing medium (1 μg/mL). Apoptosis rate was calculated from fluorescence microscope observations as the percentage of TUNEL-positive (green) cells relative to total DAPI-stained cells.

2.16 JC-1 Mitochondrial Membrane Potential Detection

A549 cells were seeded at 2×10^4 cells/well in 24-well plates, cultured for 24 h, then treated per protocol, including 10 μM cisplatin for 24 h. Cells were incubated with serum-free medium containing 10 μg/mL 5,5',6,6'-tetrachloro-1,1',3,3'-tetraethylbenzimidazolylcarbocyanine iodide (JC-1) fluorescent probe (C2006, Beyotime Institute of Biotechnology, Shanghai, China) at 37 °C for 20 min. After three gentle PBS washes to remove unbound probe, cells were observed and photographed using a fluorescence microscope under green (Ex/Em = 485/530 nm) and red (Ex/Em = 535/590 nm) channels to detect JC-1 monomers (green) and aggregates (red). ImageJ (version 1.53t, National Institutes of Health, Bethesda, MD, USA) was used to analyze the red/green fluorescence intensity ratio in each field, calculating the JC-1 monomer/aggregate ratio to assess mitochondrial membrane potential changes.

2.17 Tail-Vein-Injection Tumor Metastasis Model

Forty-two male BALB/c-nu nude mice (6–8 weeks old, 22.0 ± 2 g) were purchased from Beijing Sipeifu Biotechnology Co., Ltd. [SCXK (Jing) 2019-0004]. Housed under specific pathogen-free conditions (12 h light/dark cycle, 22 °C ± 2 °C, 55% ± 10% humidity, ad libitum food/water), mice were acclimatized for 1 week. They were then randomly divided into experimental groups (n = 6/group) using a computer-generated sequence. All animal experiments were conducted in accordance with the National Guidelines for Welfare and Ethics of Experimental Animals and the Guidelines for the Humane Treatment of Experimental Animals of China. The animal experiment met the ethical requirements, and it was approved by the Ethics Committee of The Third Affiliated Hospital of Zunyi Medical University (No. (2023)-2-295). The animals were placed in an induction chamber with 3%–4% isoflurane in oxygen until they became unconscious (approximately 3–5 min) and then transferred to a nose cone with 1.5%–2.5% isoflurane for maintenance during the procedures. The A549 cells in logarithmic growth phase after lentiviral transfection were collected. The A549 cells that were stably transfected were cultured to 80% confluence, harvested by trypsinization, and washed two times with PBS. Cell viability was confirmed to exceed 95% by trypan blue exclusion, and then 1×10^6 cells suspended in 100 μL PBS were injected via the tail vein of the control and overexpression groups. The mice were monitored daily for signs of distress, weight loss (>20% was considered endpoint), and general health status. Body weight was recorded weekly. The mice were euthanized after 6 weeks via CO_2 asphyxiation. They were placed in the euthanasia chamber without pre-charging with CO_2, and then 100% CO_2 was introduced at a fill rate of approximately 10%–30% of the chamber volume per minute. The gas was introduced appropriately to achieve gas mixture equilibrium, aiming to rapidly achieve unconsciousness and minimize animal distress. Death was confirmed by observing the absence of respiration and the fading of eye color in each rodent. CO_2 flow was maintained for a minimum of 1 min after cessation of breathing to ensure complete euthanasia. Lung tissues were collected to count visible metastatic nodules on the lung surface and for histological analysis. The lung tissues from each group of nude mice were washed with precooled PBS and fixed with 4% paraformaldehyde. After 1 week, the tissues were dehydrated, embedded in paraffin, and sectioned into 4 μm paraffin slices. Hematoxylin–eosin (HE) staining was performed in accordance with the relevant kit instructions (Beyotime Institute of Biotechnology, Shanghai, China), and the metastatic foci in the tissues were observed under an inverted microscope (Olympus, Tokyo, Japan).

2.18 Clinical Samples

Patients with lung adenocarcinoma who underwent surgical treatment at our hospital from January 2025 to April 2025 were included in this study. Twenty-five pairs of matched lung cancer tissues and adjacent normal tissues (≥5 cm from the tumor margin) were collected. The inclusion criteria were as follows: pathologically diagnosed with lung adenocarcinoma; no preoperative radiotherapy,

chemotherapy, nor other adjuvant treatments; no mediastinal lymph node metastasis nor distant organ metastasis; and complete clinical, pathological, and imaging data. The exclusion criteria were as follows: presence of other pulmonary diseases such as pneumonia or congenital pulmonary diseases; malignant tumors in other sites; history of thoracic surgery; and comorbid heart, brain, liver, or kidney diseases or other systemic diseases. A total of 25 patients were ultimately included, comprising 16 males and nine females aged 48–76 years, with a mean age of 62.1 ± 9.8 years. This study involving human participants was conducted in accordance with the Declaration of Helsinki. This study was approved by the hospital Ethics Committee of The Eighth Affiliated Hospital, Southern Medical University (The First People's Hospital of Shunde Foshan) (Approval No. 20250106-116). All patients voluntarily participated and signed informed consent forms.

2.19 Immunohistochemical Staining

Paraffin-embedded tissues were sectioned at 4 µm, deparaffinized with xylene, and rehydrated with graded ethanol (100%, 95%, 75%, and 50%). After Ethylenediaminetetraacetic acid (EDTA) (Thermo Fisher Scientific, Waltham, MA, USA) antigen retrieval, endogenous peroxidase was quenched with 3% hydrogen peroxide. Sections were blocked with 4% BSA (30 min, room temperature), then incubated overnight at 4 °C with primary PTDSS1 antibody (1:200; ab157222, Abcam, Cambridge, UK). Following PBS washes, secondary antibody incubation (60 min, room temperature) and 3,3'-Diaminobenzidine (DAB) staining were performed. Sections were counterstained with hematoxylin, blued, dehydrated with graded alcohol and xylene, then mounted. Staining intensity was evaluated by three pathologists across five high-power fields (×200) per section based on positive cell percentage (<5% = 0, 5–25% = 1, 26–50% = 2, 51–75% = 3, 76–100% = 4) and intensity (no staining = 0, light yellow = 1, brown-yellow = 2, dark brown = 3). Final scores (percentage × intensity) were categorized: negative (0), weak positive (1–4), positive (5–8), or strong positive (9–12).

2.20 Statistical Analysis

Data are presented as mean ± standard deviation. Statistical analyses were performed using GraphPad Prism (version 10.0, GraphPad Software, San Diego, CA, USA). Student's *t*-test was used for two-group comparisons, while one-way ANOVA with Tukey's multiple comparison test was used for multiple groups. Survival curves were generated by Kaplan-Meier method, and differences analyzed by log-rank test. Pearson's correlation analyzed gene expression. $p < 0.05$ was considered statistically significant. All *in vitro* experiments were repeated at least three times.

3. Results

3.1 PTDSS1 is an Oncogene Associated With Lung Cancer Progression and Poor Clinical Prognosis

PTDSS1 co-expressed proteins were first analyzed using the LinkedOmics database to investigate the expression characteristics and clinical significance of PTDSS1 in lung cancer. The volcano plot displays proteins associated with PTDSS1 expression (Fig. 1A), followed by cluster analysis identifying protein groups positively (Fig. 1B) and negatively (Fig. 1C) correlated with PTDSS1. Transcriptome data from patients with lung cancer in TCGA database were analyzed to validate the PTDSS1 expression levels in lung cancer. The results demonstrated upregulated *PTDSS1* mRNA expression levels in the lung cancer tissues (Fig. 1D). Kaplan-Meier survival analysis showed patients with high PTDSS1 expression had shorter overall survival (Fig. 1E). Analysis of the TCGA database revealed that *PTDSS1* expression levels positively correlate with lymph node metastasis (N stage) in lung cancer (Fig. 1F). Specifically, patients at N2 stage exhibited higher *PTDSS1* expression levels than patients at N0-1 stage, indicating that *PTDSS1* may promote lymph node metastasis in lung cancer and participate in malignant tumor progression. The PTDSS1 protein expression levels in 25 paired lung cancer tissues and adjacent normal tissues were detected using immunohistochemistry to further validate the PTDSS1 expression characteristics in lung cancer. The results showed higher PTDSS1 staining intensity in the lung cancer tissues than in the paired adjacent normal tissues (Fig. 1G).

3.2 PTDSS1 Promotes In Vitro Proliferation and Metastasis of Lung Cancer Cells

Western blot analysis demonstrated that the A549 and NCI-H1299 cells transfected with OE-PTDSS1 plasmid had an increase in PTDSS1 protein expression levels compared with the control group (OE-NC, Fig. 2A and **Supplementary Fig. 2**), confirming successful construction of the overexpression model. PTDSS1 overexpression significantly enhanced the proliferative capacity of A549 and NCI-H1299 cells, as demonstrated by increased CCK-8 activity and EdU-positive cell percentage and enhanced colony formation ability compared with the controls (Fig. 2B–D). Transwell invasion assay results showed that PTDSS1 overexpression increased the number of A549 and NCI-H1299 cells penetrating through the Matrigel matrix (Fig. 2E), indicating that PTDSS1 enhances the invasive capacity of lung cancer cells. Cytoskeletal staining revealed that the A549 and NCI-H1299 cells in the PTDSS1 overexpression group exhibited typical spindle-shaped morphology with increased cell length (Fig. 2F). A tail-vein-injection tumor metastasis model was established to validate whether the *in vitro* findings of PTDSS1 promoting lung cancer metastasis are consistent *in vivo*. The A549 and NCI-H1299 cells overexpressing PTDSS1 or control

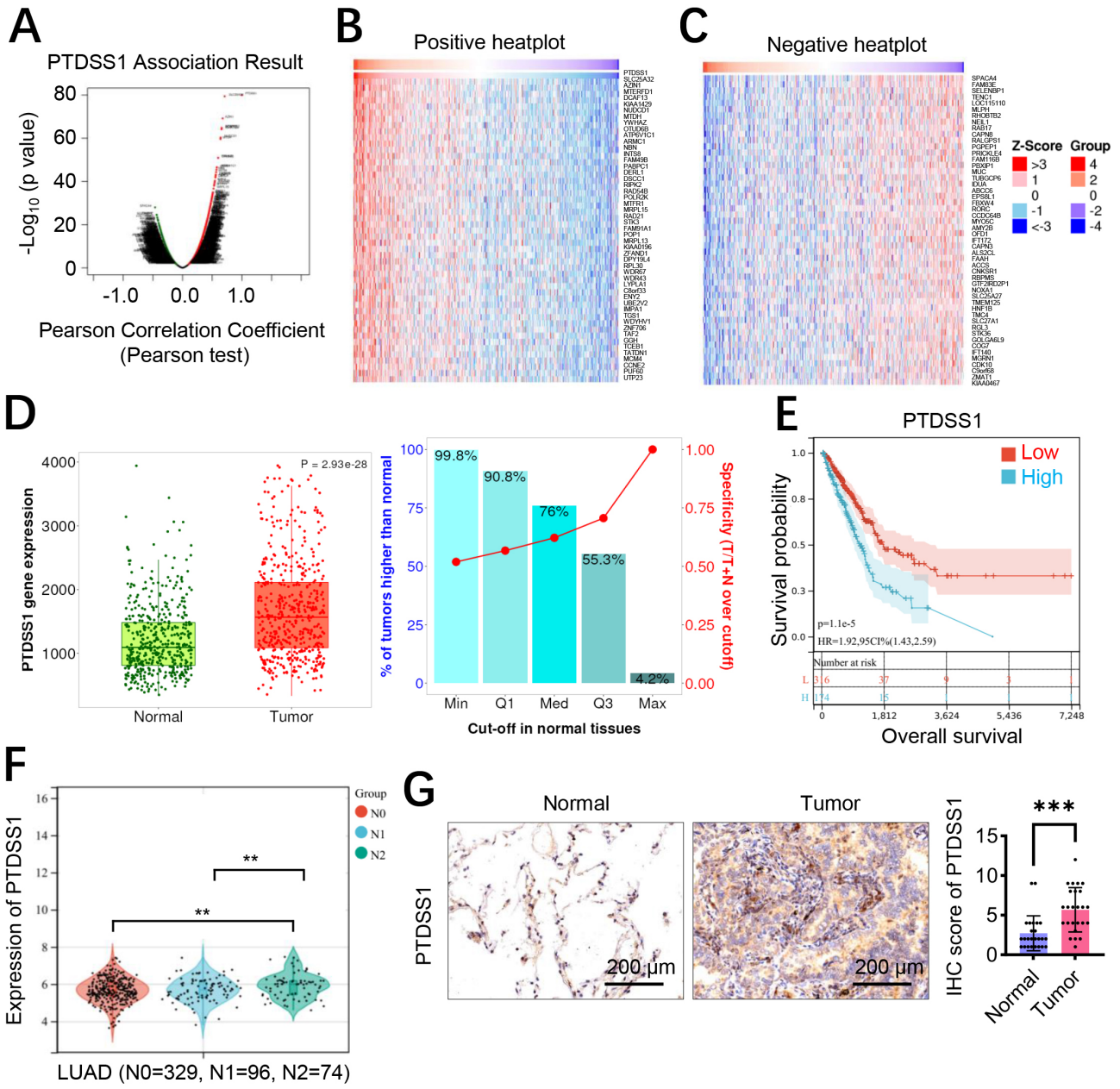

Fig. 1. PTDSS1 is an oncogene associated with lung cancer progression and poor clinical prognosis. (A–C) LinkedOmics database analysis of PTDSS1 co-expression correlation proteins. (A) Volcano plot of PTDSS1 co-expressed proteins (X-axis: Pearson Correlation Coefficient; Y-axis: -log10 *p*-value). (B) Cluster analysis of proteins positively correlated with PTDSS1 (Groups: functional protein clusters based on correlation coefficients >0.3). (C) Cluster analysis of proteins negatively correlated with PTDSS1 (Groups: functional protein clusters based on correlation coefficients <–0.3). (D) Analysis of PTDSS1 expression in lung cancer tumor tissues versus adjacent tissues in TCGA (Y-axis: PTDSS1 expression level, log2 TPM+1 (TPM: Transcripts Per Million); quantification represents mean ± SEM (Standard Error of the Mean) from TCGA dataset analysis). (E) Kaplan-Meier survival analysis of lung cancer patients based on PTDSS1 expression levels from TCGA database (X-axis: Overall survival time in days; Y-axis: Survival probability). (F) Correlation analysis between PTDSS1 expression in lung cancer tumor tissues and pathological N stage in TCGA (X-axis: N stage classification (N0, N1, N2); Y-axis: PTDSS1 expression level, log2 TPM+1). (G) Immunohistochemical detection and quantitative analysis of PTDSS1 expression in adjacent normal tissues and paired tumor samples (Scale bar: 50 μm; quantification shows relative staining intensity). Data were presented as means ± SEM, $^{**}p < 0.01$, $^{***}p < 0.001$. PTDSS1, phosphatidylserine synthase 1; TCGA, The Cancer Genome Atlas; LUAD, Lung Adenocarcinoma.

plasmid were injected into the tail veins of BALB/c nude mice, and lung metastasis was evaluated after 6 weeks. The histopathological analysis showed an increased number of metastatic foci in the lung tissues of the PTDSS1 overexpression group (Fig. 2G). An increase in the number of micrometastatic lesions was observed in the lung tissues of the PTDSS1 overexpression group, exhibiting distinct infiltrative growth characteristics. SiRNA-mediated knockdown was performed in the A549 and NCI-H1299 cells to validate PTDSS1 function. PTDSS1 silencing significantly reduced cell proliferation (EdU assays: ~50% reduction, $p < 0.01$), colony formation capacity (~70% reduction, $p < 0.001$), and migration ability (~60% reduction, $p < 0.01$) compared with the control siRNA in both cell lines (**Supplementary Fig. 1**). These loss-of-function results confirmed that PTDSS1 knockdown reverses the oncogenic phenotypes observed in overexpression studies.

3.3 PTDSS1 Promotes Aerobic Glycolysis in Lung Cancer In Vitro

Bioinformatic enrichment analysis of PTDSS1 co-expressed genes showed significant enrichment in energy metabolism-related pathways (Fig. 3A), suggesting the involvement of PTDSS1 in metabolic reprogramming of lung cancer. The effect of PTDSS1 on the expression levels of key glycolytic enzymes was further examined. RT-qPCR analysis revealed that *PTDSS1* overexpression upregulated the mRNA expression levels of multiple key glycolytic enzymes in the A549 and NCI-H1299 cells. Specifically, lactate dehydrogenase A (*LDHA*, Fig. 3B), glucose transporter 1 (*GLUT1*, Fig. 3C), *PKM2* (Fig. 3D), and phosphofructokinase muscle type (*PFKM*, Fig. 3E) showed upregulation in the PTDSS1 overexpression group. Cellular OCR and ECAR were measured using the Seahorse cellular energy metabolism analyzer to directly assess the impact of PTDSS1 on the metabolic phenotype of lung cancer cells. The OCR results showed that PTDSS1 overexpression reduced the basal respiration and maximum respiratory capacity of NCI-H1299 and A549 cells (Fig. 3F), indicating that PTDSS1 overexpression inhibited mitochondrial oxidative phosphorylation. Conversely, the ECAR measurement results showed that glycolysis rate and glycolytic capacity were higher in the PTDSS1 overexpression group than in the control group (Fig. 3G), indicating that PTDSS1 promoted glycolytic activity in lung cancer cells. PTDSS1 overexpression increased glucose uptake (Fig. 3H) and lactate secretion (Fig. 3I) in the NCI-H1299 and A549 cells. These results demonstrated that PTDSS1 promotes glucose uptake and utilization in lung cancer cells, enhancing aerobic glycolytic activity. Pearson's correlation analysis showed that *PTDSS1* expression positively correlated with *PKM2*, *PFKM*, *LDHA*, and *GLUT1* in clinical lung cancer samples (Fig. 3J), supporting PTDSS1's role in glycolytic reprogramming.

3.4 Nuclear PTDSS1 Plays a Critical Role in Promoting Lung Cancer Progression Through Glycolysis

On the basis of previous findings that PTDSS1 promotes glycolysis and malignant progression in lung cancer, and the important role of nuclear proteins in metabolic regulation in recent years, this study hypothesized that PTDSS1 may possess subcellular compartment-specific functions. A PTDSS1 overexpression vector with a nuclear localization signal peptide (NLS-PTDSS1), directing PTDSS1 specifically to the nucleus, was constructed to verify this hypothesis. Immunofluorescence was conducted to validate the successful construction of the experimental model. Compared with the control group and the full-length PTDSS1 overexpression group (OE-PTDSS1^{All}), the A549 cells transfected with NLS-PTDSS1 (OE-PTDSS1^{N}) displayed significantly enhanced nuclear PTDSS1 fluorescence signals, primarily localized within the nucleus (Fig. 4A). The results showed that glucose uptake and lactate secretion increased in the OE-PTDSS1^{All} group. The glucose uptake (Fig. 4B) and lactate secretion (Fig. 4C) levels in the OE-PTDSS1^{N} group further increased, exceeding those in the OE-PTDSS1^{All} group. The EdU incorporation assay results showed an increase in the EdU-positive rate of the OE-PTDSS1^{All} group. The EdU-positive rate of the OE-PTDSS1^{N} group further increased, exceeding that of the OE-PTDSS1^{All} group (Fig. 4D). The colony formation assays further confirmed that the OE-PTDSS1^{N} group exhibited stronger colony-forming ability than the OE-PTDSS1^{All} and control groups (Fig. 4E). These results indicated that nuclear PTDSS1 effectively promotes lung cancer cell proliferation, possibly due to its enhanced glycolysis regulatory capability. The OE-PTDSS1^{N} group exhibited more prominent spindle-shaped morphology and increased cell length than the OE-PTDSS1^{All} group (Fig. 4F). A lung metastasis model was established by injecting the three treatment groups of A549 cells into the tail veins of BALB/c nude mice to validate the role of nuclear PTDSS1 in promoting tumor metastasis *in vivo*. The pathological analysis results after 6 weeks showed an increase in the number of metastatic foci in the lung tissues of the OE-PTDSS1^{N} group compared with that in the control and OE-PTDSS1^{All} groups (Fig. 4G). More and larger micrometastatic lesions were observed in the lung tissues of the OE-PTDSS1^{N} group, exhibiting a more pronounced invasive growth pattern.

3.5 PTDSS1 Accelerates Glycolysis Through PKM2

The functional relationship of PTDSS1 and PKM2 was investigated given the co-expression correlation between them. Immunofluorescence showed co-localization of PTDSS1 and PKM2 in the A549 cells (Fig. 5A). The PKM2 in PTDSS1-overexpressing cells was silenced to examine PKM2's role in PTDSS1-mediated glycolysis. The metabolic analysis revealed that PTDSS1 overexpression increased glucose uptake (Fig. 5B) and lactate secretion

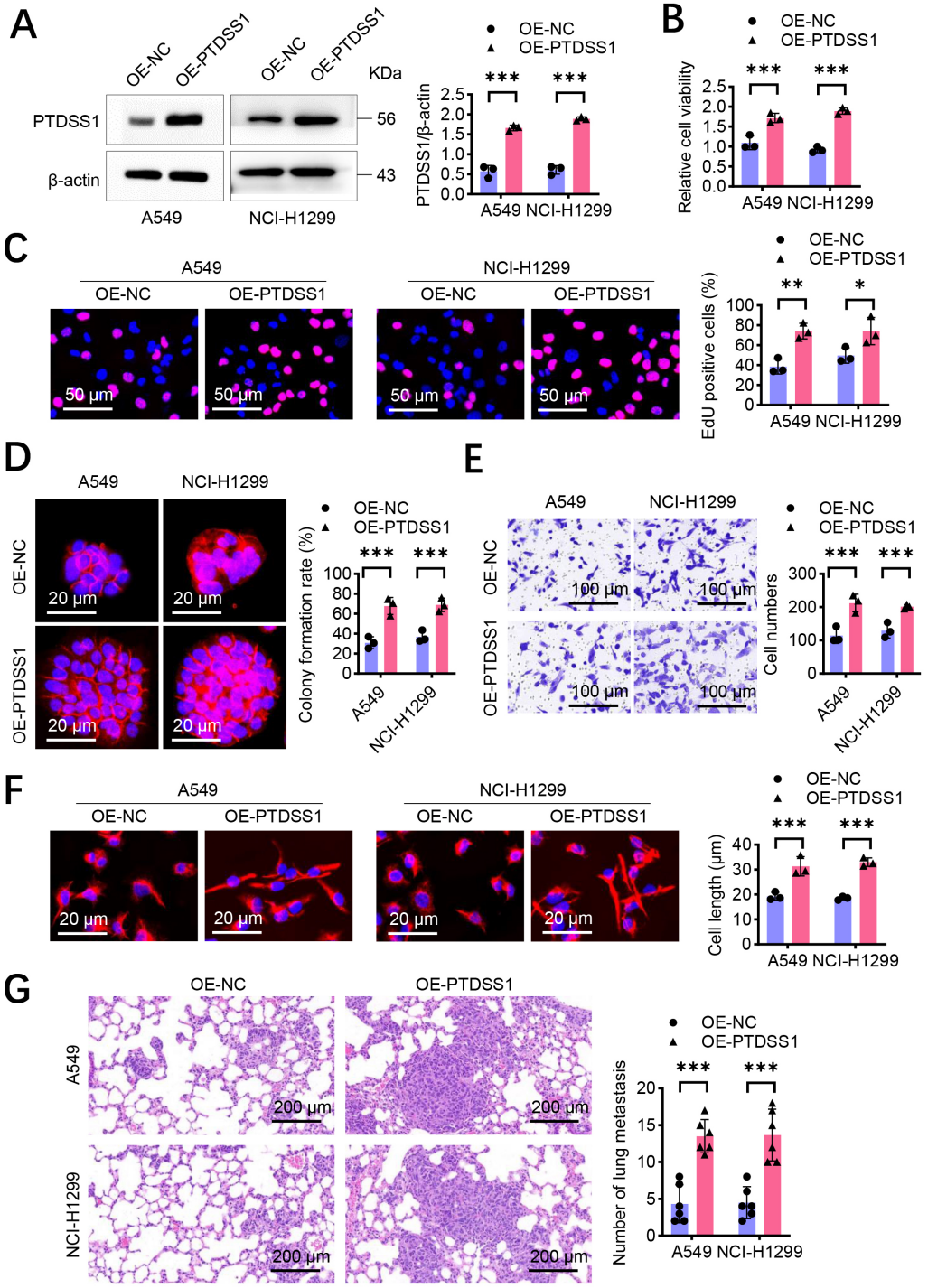

Fig. 2. PTDSS1 promotes proliferation and metastasis of lung cancer cells *in vitro*. (A) Western blot detection of transfection efficiency in A549 and NCI-H1299 cells transfected with control vector OE-NC and overexpression plasmid (OE-PTDSS1). (B) CCK-8 detection of cell viability in A549 and NCI-H1299 cells after PTDSS1 overexpression. (C) 5-ethyl-2'-deoxyuridine (EdU) detection of proliferation capacity in A549 and NCI-H1299 cells after PTDSS1 overexpression. Scale bar: 50 μm. (D) Colony formation assay measuring proliferation capacity in A549 and NCI-H1299 cells after PTDSS1 overexpression, Y-axis: Clone formation efficiency (% of seeded cells). Scale bar: 20 μm. (E) Transwell invasion assay evaluating invasive capacity in A549 and NCI-H1299 cells after PTDSS1 overexpression. Scale bar: 100 μm. (F) Cytoskeletal staining in NCI-H1299 and A549 cells demonstrating disappearance of spindle morphology and shortened cell length after PTDSS1 overexpression. Scale bar: 20 μm. (G) Establishment of tail vein injection tumor metastasis model in BALB/c nude mice (n = 6) using PTDSS1-overexpressing A549 and NCI-H1299 cells. Scale bar: 200 μm. Data were presented as means ± SEM. N = 3, *$p < 0.05$, **$p < 0.01$, ***$p < 0.001$. OE-OC, overexpression negative control; CCK-8, cell counting kit-8.

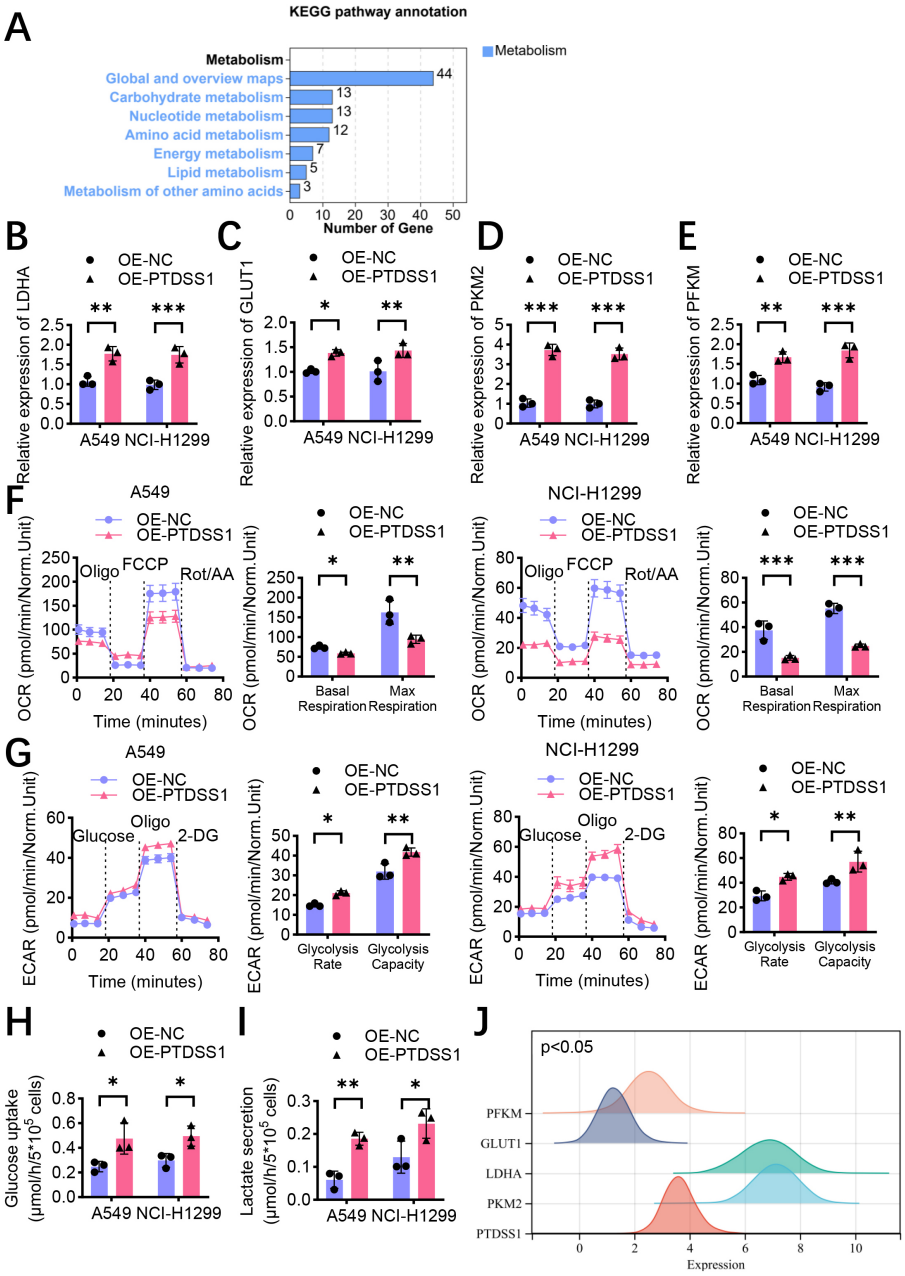

Fig. 3. PTDSS1 promotes aerobic glycolysis in lung cancer *in vitro*. (A) Enrichment analysis of PTDSS1 co-expressed genes shows significant enrichment in energy metabolism-related pathways and functions. (B) RT-qPCR detection of relative mRNA expression levels of glycolysis-related gene *LDHA* in control and stable PTDSS1-overexpressing A549 and NCI-H1299 cells. (C) RT-qPCR detection of relative mRNA expression levels of glycolysis-related gene *GLUT1* in control and stable PTDSS1-overexpressing A549 and NCI-H1299 cells. (D) RT-qPCR detection of relative mRNA expression levels of glycolysis-related gene *PKM2* in control and stable PTDSS1-overexpressing A549 and NCI-H1299 cells. (E) RT-qPCR detection of relative mRNA expression levels of glycolysis-related gene *PFKM* in control and stable PTDSS1-overexpressing A549 and NCI-H1299 cells. (F) Measurement of oxygen consumption rate (OCR) in control and stable PTDSS1-overexpressing NCI-H1299 and A549 cells. Analysis of basal respiration and maximal respiration. (G) Measurement of extracellular acidification rate (ECAR) in control and PTDSS1-overexpressing NCI-H1299 and A549 cells. Analysis of glycolytic rate and glycolytic capacity. (H) Detection of glucose uptake in control and stable PTDSS1-overexpressing NCI-H1299 and A549 cells. (I) Detection of lactate secretion in control and stable PTDSS1-overexpressing NCI-H1299 and A549 cells. (J) Ridge plot analysis showing expression distribution patterns of PTDSS1 and key glycolysis-related genes (*PKM2*, *PFKM*, *LDHA*, and *GLUT1*) in lung cancer patients from TCGA dataset (X-axis: Gene expression level, log2 TPM+1; Y-axis: Gene names; density curves show expression distribution for each gene). Data were presented as means ± SEM. N = 3, $*p < 0.05$, $**p < 0.01$, $***p < 0.001$. *LDHA*, lactate dehydrogenase A; *GLUT1*, glucose transporter 1; *PFKM*, phosphofructokinase muscle type.

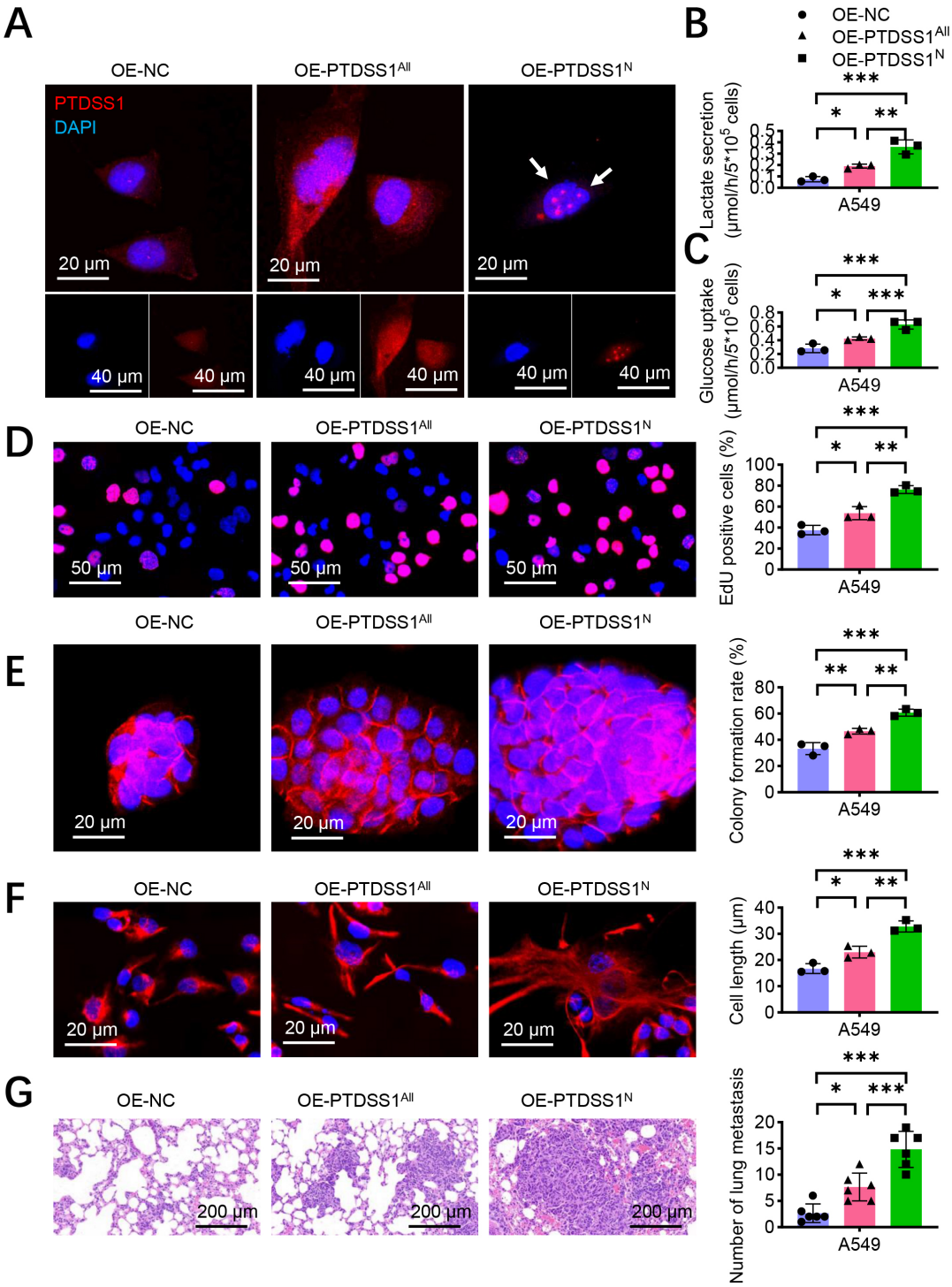

Fig. 4. Nuclear PTDSS1 plays a more critical role in promoting lung cancer progression through glycolysis. (A) Construction of PTDSS1 nuclear localization signal peptide (NLS-PTDSS1) transfected in A549 cells, with immunofluorescence detection of PTDSS1 localization. Scale bar: 20 μm (upper); scale bar: 40 μm (lower). (B) Detection of glucose uptake in control and stable PTDSS1-overexpressing A549 cells. (C) Detection of lactate secretion in control and stable PTDSS1-overexpressing A549 cells. (D) EdU assay evaluating proliferation capacity in control and stable PTDSS1-overexpressing A549 cells. Scale bar: 50 μm. (E) Colony formation assay examining proliferation capacity in control and stable PTDSS1-overexpressing A549 cells. Scale bar: 20 μm. (F) Detection of cytoskeletal changes in control and stable PTDSS1-overexpressing A549 cells. Scale bar: 20 μm. (G) Establishment of tail vein injection tumor metastasis model in BALB/c nude mice (n = 6) using control and stable PTDSS1-overexpressing A549 cells. Scale bar: 200 μm. Data were presented as means ± SEM. N = 3, *$p < 0.05$, **$p < 0.01$, ***$p < 0.001$. DAPI, 4',6-diamidino-2-phenylindole.

(Fig. 5C) compared with control treatment. However, simultaneous silencing of PKM2 with PTDSS1 overexpression (OE-PTDSS1 + shPKM2) reversed the promotive effect of PTDSS1 on glucose uptake and lactate secretion. This result indicated that PTDSS1's promotion of glycolysis primarily depends on PKM2. Subsequently, the role of PKM2 in PTDSS1-promoted lung cancer cell proliferation was assessed. PTDSS1 overexpression increased the DNA synthesis activity in A549 cells (Fig. 5D), whereas silencing PKM2 inhibited this pro-proliferative effect. PTDSS1 overexpression significantly enhanced the colony formation ability of A549 cells, and silencing PKM2 effectively blocked this effect (Fig. 5E). These results indicated that PKM2 is a key molecule mediating the pro-proliferative effects of PTDSS1. Moreover, PTDSS1 overexpression caused the A549 cells to transform toward a spindle shape with increased cell length, whereas silencing PKM2 in the PTDSS1-overexpressing cells reduced cell length (Fig. 5F), suggesting that PKM2 also plays an important role in PTDSS1-promoted cell invasion and metastatic potential. The PTDSS1-overexpressing A549 cells were treated with the glycolysis inhibitor 2-DG to further verify the critical role of glycolysis in PTDSS1-promoted malignant phenotypes in lung cancer. The results showed that compared with control treatment, 2-DG treatment inhibited the PTDSS1 overexpression-induced increase in glucose uptake (Fig. 5G) and enhanced lactate secretion (Fig. 5H), confirming that 2-DG effectively inhibits PTDSS1-promoted glycolytic activity. Furthermore, 2-DG treatment reversed the PTDSS1-enhanced proliferation (EdU assays), colony formation, and morphological changes in A549 cells (Fig. 5I–K), indicating that glycolysis inhibition blocks PTDSS1's oncogenic effects and confirming glycolysis as a key pathway for PTDSS1-mediated malignant progression.

3.6 PTDSS1 Maintains Mitochondrial Homeostasis and Inhibits Oxidative Phosphorylation and Apoptosis in Lung Cancer Cells

Mitotracker staining showed significant co-localization of PTDSS1 with the mitochondria (Fig. 6A). The TUNEL assays revealed that PTDSS1 overexpression reduced cisplatin-induced apoptosis in the A549 and NCI-H1299 cells compared with control treatment (Fig. 6B), suggesting that PTDSS1 enhances apoptosis resistance through mitochondrial function regulation. A key marker of the mitochondrion-mediated apoptosis pathway is the release of cytochrome c (Cyt c) from the mitochondria to the cytoplasm. Cytoplasmic and mitochondrial fractions were separated, and the distribution of Cyt c after cisplatin treatment was examined to confirm the effect of PTDSS1 on the mitochondrial apoptosis pathway. The results showed that the PTDSS1 overexpression group had reduced Cyt c levels in the cytoplasm while maintaining higher levels of Cyt c in the mitochondria (Fig. 6C). This result indicated that PTDSS1 can prevent the release of Cyt c from the mitochondria to the cytoplasm, thereby inhibiting the activation of the mitochondrion-dependent apoptosis pathway. Considering PTDSS1's role in promoting glycolysis, the relationship between glycolysis and PTDSS1-maintained mitochondrial homeostasis was further explored. By treating PTDSS1-overexpressing A549 cells with 2-DG, PTDSS1's protective effect against cisplatin-induced apoptosis was attenuated (Fig. 6D). The TUNEL staining showed that the apoptosis rate in the 2-DG treatment group (OE-PTDSS1 + 2-DG) was higher than that in the control group. This result indicated that PTDSS1 inhibits lung cancer cell apoptosis by promoting glycolysis. The analysis of JC-1 fluorescent probe found that PTDSS1 overexpression could maintain mitochondrial membrane potential in A549 cells after cisplatin treatment, manifested as enhanced red fluorescence (J-aggregates) and reduced green fluorescence (J-monomers). Meanwhile, 2-DG treatment reversed PTDSS1's protective effect, resulting in an increase in JC-1 monomer/aggregate ratio (Fig. 6E), indicating decreased mitochondrial membrane potential and impaired mitochondrial function. This result further confirmed that PTDSS1 maintains mitochondrial functional homeostasis by promoting glycolysis. The expression levels of factors related to mitochondrial biogenesis and dynamics were examined to explore the molecular mechanisms by which PTDSS1 maintains mitochondrial homeostasis. RT-qPCR showed that PTDSS1 overexpression upregulated the mitochondrial biogenesis regulator *PGC-1*α and the fusion proteins *MFN1/MFN2*, which were inhibited by 2-DG treatment (Fig. 6F–H). These results suggest that PTDSS1 maintains mitochondrial homeostasis by promoting biogenesis and fusion, thereby inhibiting mitochondrion-dependent apoptosis.

3.7 PTDSS1 Exhibits Co-expression Correlation With Glycolytic Pathway-Related Protein PKM2

Immunohistochemistry of 25 paired lung cancer and adjacent normal tissues showed enhanced PKM2 staining in cancer tissues (Fig. 7A,B). Correlation analysis was performed between PTDSS1 and PKM2 protein expression levels in these tumor samples. As shown in Fig. 7C, the expression levels of PTDSS1 and PKM2 in tumor tissues were positively correlated ($r^2 = 0.234$, $p < 0.014$). The RNA-seq data from 501 patients with lung cancer in TCGA database were analyzed to further validate these results. As shown in Fig. 7D, the large-sample analysis similarly supported a positive correlation between PTDSS1 and PKM2 at the mRNA level. These results consistently indicated that PTDSS1 and PKM2 maintain a robust co-expression relationship in lung cancer, further supporting the mechanism revealed by previous functional experiments, i.e., PTDSS1 regulates glycolysis through PKM2. On the basis of all experimental results from the present study, a mechanistic model of PTDSS1 regulating mitochondrial homeostasis

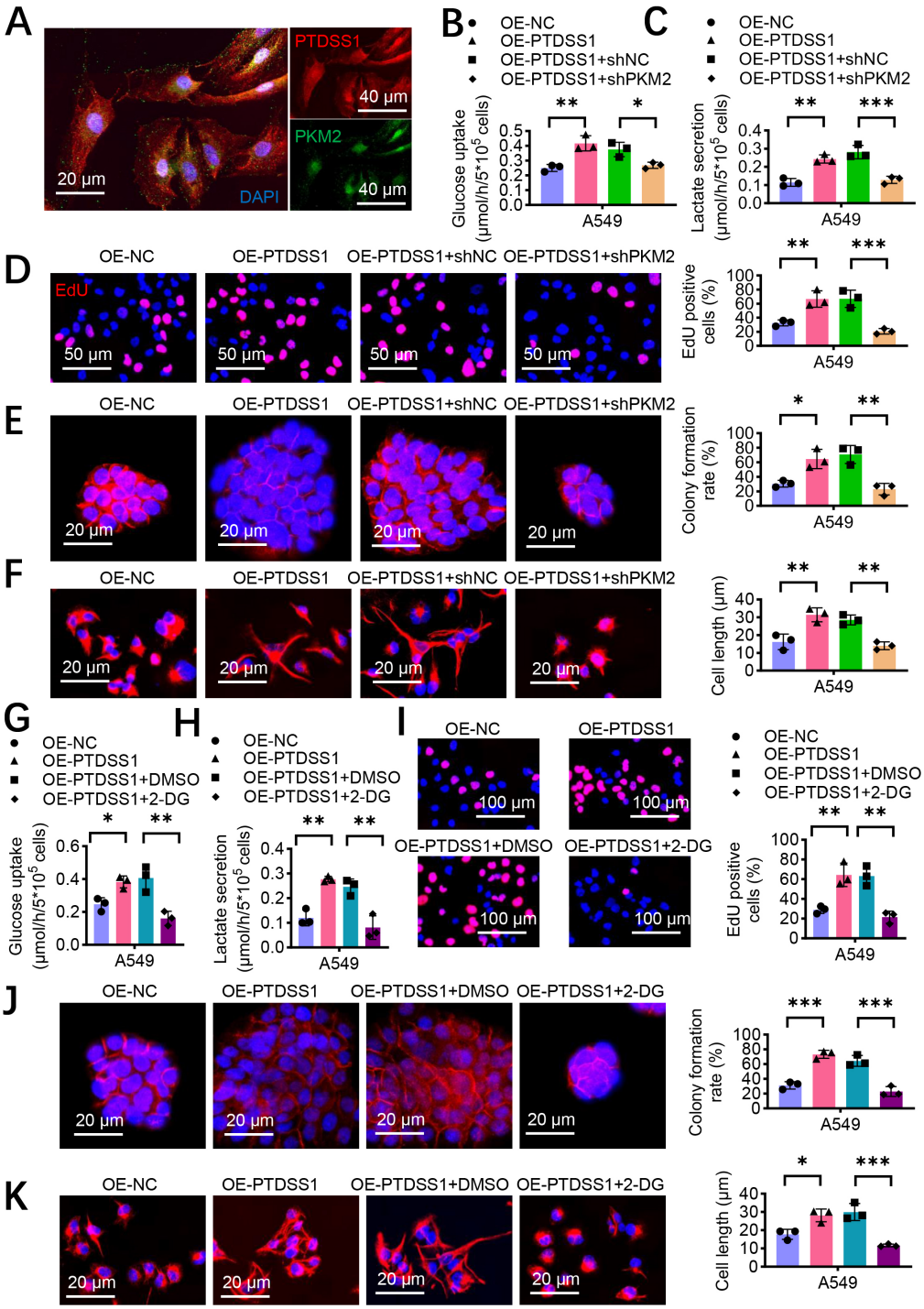

Fig. 5. PTDSS1 accelerates glycolysis through PKM2. (A) Representative images of PTDSS1 and PKM2 co-localization in A549 cells. Scale bar: 20 um (left); scale bar: 40 um (right) . (B) Silencing PKM2 reduces the promoting effect of PTDSS1 on glucose uptake in A549 cells. (C) Silencing PKM2 reduces the promoting effect of PTDSS1 on lactate secretion in A549 cells. (D) EdU assay examining proliferation capacity in A549 cells with different treatments. Scale bar: 50 μm. (E) Colony formation assay evaluating proliferation capacity in A549 cells with different treatments. Scale bar: 20 μm. (F) Detection of cytoskeletal changes in A549 cells with different treatments. Scale bar: 20 μm. (G) Glycolysis inhibitor 2-DG treatment inhibits the promoting effect of PTDSS1 on glucose uptake in A549 cells. (H) Glycolysis inhibitor 2-DG treatment inhibits the promoting effect of PTDSS1 on lactate secretion in A549 cells. (I) EdU assay evaluating proliferation capacity in A549 cells with different treatments. Scale bar: 100 μm. (J) Colony formation assay examining proliferation capacity in A549 cells with different treatments. Scale bar: 20 μm. (K) Detection of cytoskeletal changes in A549 cells with different treatments. Scale bar: 20 μm. Data were presented as means ± SEM. N = 3, *$p < 0.05$, **$p < 0.01$, ***$p < 0.001$.

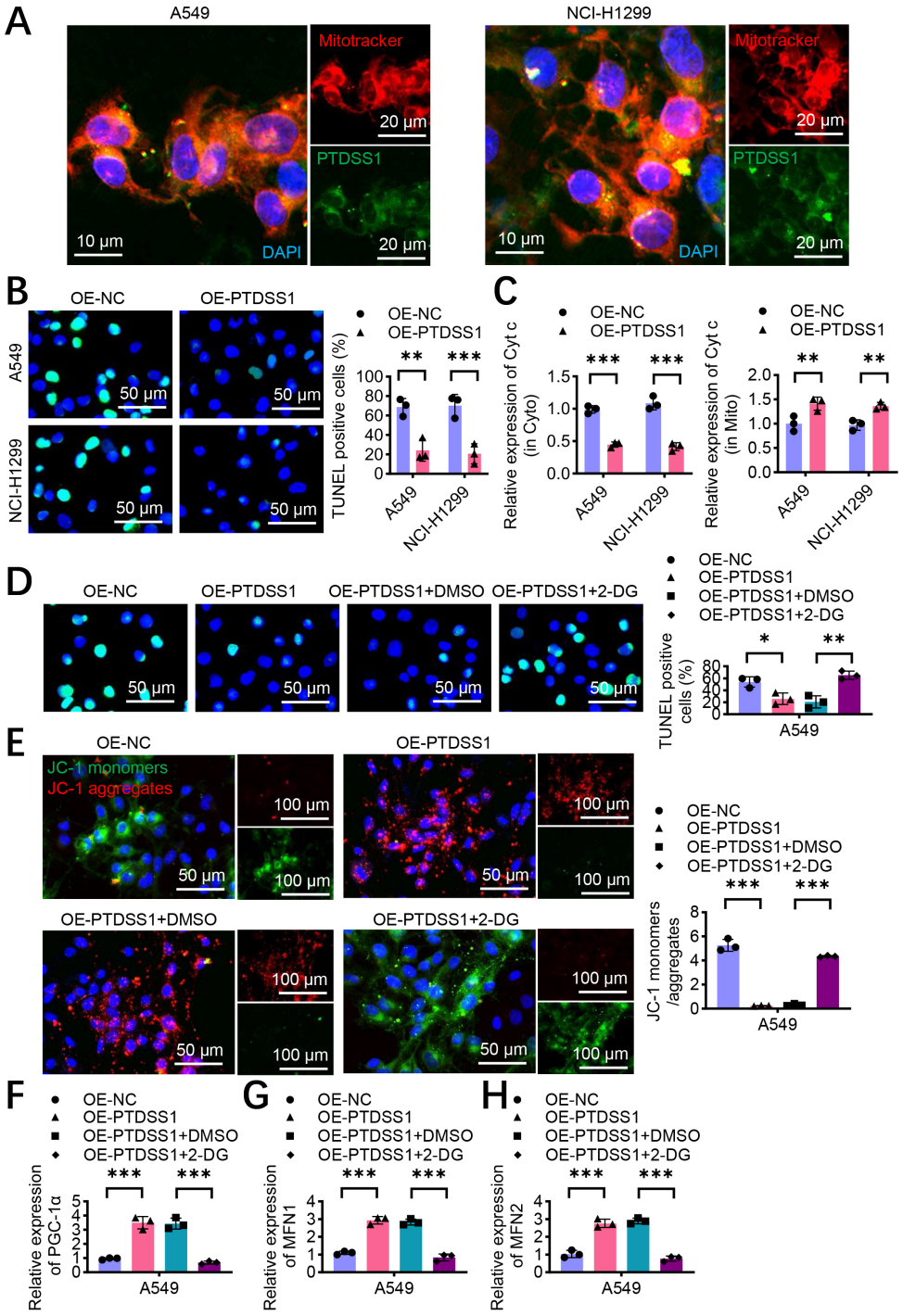

Fig. 6. PTDSS1 maintains mitochondrial homeostasis and inhibits oxidative phosphorylation and apoptosis in lung cancer cells. (A) Immunofluorescence co-localization analysis of PTDSS1 and mitochondria in A549 and NCI-H1299 cells. Cells were stained with MitoTracker Red (mitochondrial marker, red fluorescence) and anti-PTDSS1 antibody (green fluorescence), with DAPI for nuclear counterstaining (blue fluorescence). Scale bar: 10 um (left); scale bar: 20 um (right). (B) Terminal deoxynucleotidyl transferase dUTP nick end labeling (TUNEL) analysis of apoptosis in A549 and NCI-H1299 cells after cisplatin treatment (10 μM, 24 hours). Scale bar: 50 μm. (C) PTDSS1 inhibits cytoplasmic Cyt c expression, maintains mitochondrial Cyt c expression, and suppresses oxidative phosphorylation (cisplatin treatment, 10 μM, 24 hours). (D) TUNEL assay examining apoptosis in A549 cells with different treatments. Scale bar: 50 μm. (E) JC-1 fluorescent probe detection of mitochondrial membrane potential in A549 cells with different treatments. Scale bar: 50 μm (left); scale bar: 100 μm (right). (F–H) PCR analysis of *PGC-1α* (F), *MFN1* (G), and *MFN2* (H) expression levels in A549 cells with different treatments. Data were presented as means ± SEM. N = 3, *$p < 0.05$, **$p < 0.01$, ***$p < 0.001$. Cyt c, cytochrome c.

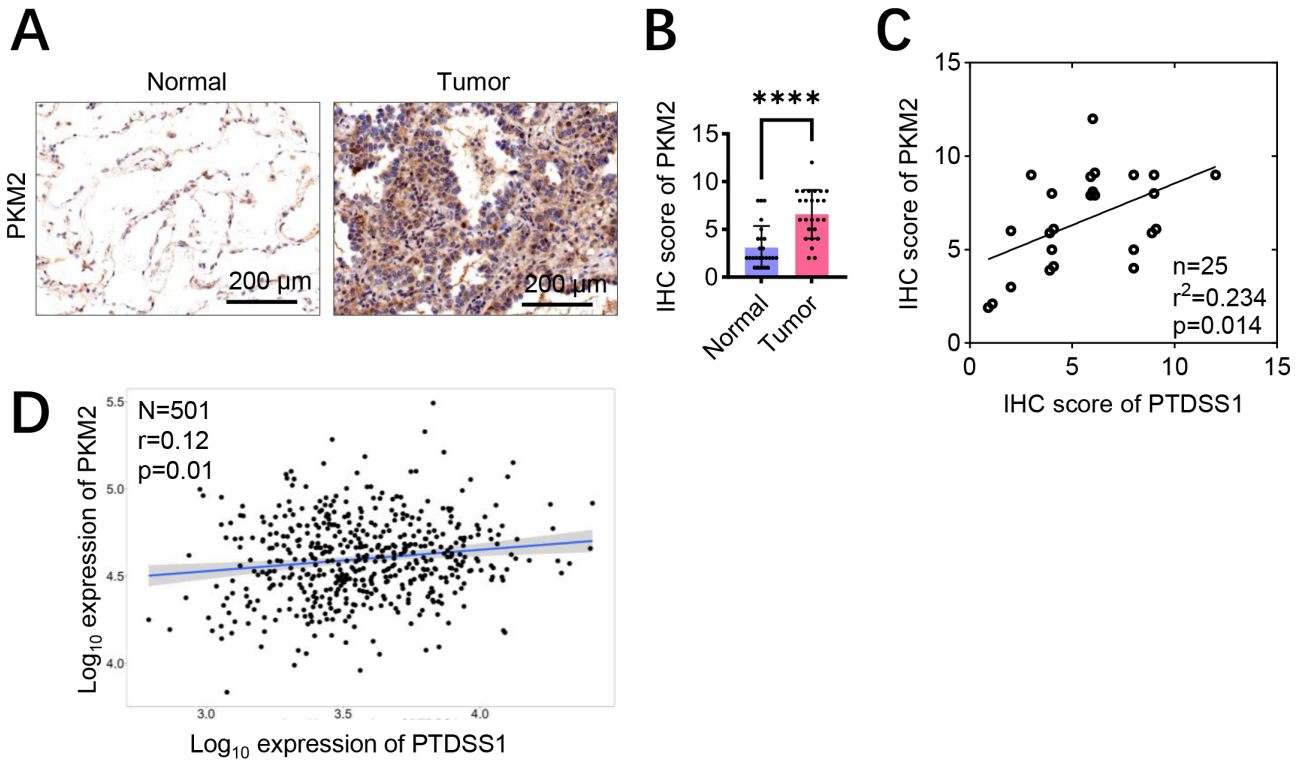

Fig. 7. PTDSS1 exhibits co-expression correlation with glycolysis pathway-related proteins. (A,B) Assessment of PKM2 protein levels in lung cancer patient specimens by immunohistochemistry (IHC) staining. Scale bar: 200 μm (A). (C) Positive correlation of PTDSS1 and PKM2 co-expression in tumor tissues from 25 patients (Data points were jittered slightly (±0.1) to display all 25 patients clearly). (D) TCGA database analysis showing positive correlation between PTDSS1 and PKM2 co-expression in lung cancer patients (n = 501). Data were presented as means ± SEM. ****$p < 0.0001$.

and thus driving glycolysis and lung cancer progression was proposed (Fig. 8). This model elucidated that PTDSS1 is upregulated in lung cancer and coordinately regulates cellular metabolism and survival through nuclear and mitochondrial compartment-specific actions.

4. Discussion

This study provides evidence that PTDSS1, a PS synthesis enzyme, correlates with malignant progression in lung cancer and shows associations with altered cellular metabolism. While PTDSS1 has been traditionally studied for its role in membrane phospholipid synthesis [10], the findings of the present study suggest potential connections to metabolic regulation in lung cancer, expanding the functional scope of this enzyme beyond its canonical lipid biosynthetic role. The results demonstrated that PTDSS1 upregulation in lung cancer tissues correlates with enhanced cellular proliferation and metabolic alterations, particularly increased glycolytic activity. This observation aligns with emerging evidence highlighting the multifaceted roles of lipid metabolism enzymes in tumor progression [8].

Research indicates that PTDSS1 participates in multiple biological processes, including cell membrane assembly, apoptosis, immune regulation, and neural development

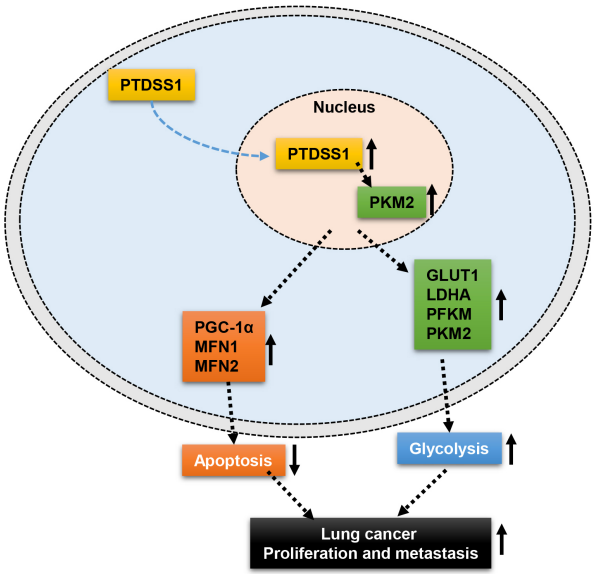

Fig. 8. Schematic diagram illustrating the current hypothesis of the mechanism by which PTDSS1 may regulate mitochondrial homeostasis, drive glycolysis, and promote lung cancer progression. ↑, indicates upregulated expression or enhanced function; ↓, indicates downregulated function.

[26]. PTDSS1 plays a key role in cell membrane assembly by catalyzing the conversion of PS to phosphatidylcholine (PC), an essential component of cell membranes [27]. Studies have shown that PTDSS1 deficiency or dysfunction can lead to abnormal cell membrane assembly, thereby affecting cellular function. Additionally, PTDSS1 plays an important role in the apoptosis process [10]. Apoptosis is a normal mode of cell death, and PTDSS1 participates in apoptotic signal transduction by regulating PS content on the cell membrane. Research has found that PTDSS1 deficiency can lead to abnormal transmission of apoptotic signals, thereby affecting cell survival and death decisions. PTDSS1 also participates in immune regulation processes [28]. Studies have shown that PTDSS1 plays an important role in lymphocyte activation and differentiation. PTDSS1 deficiency can lead to immune cell dysfunction, potentially causing immune system dysregulation and increasing the risk of autoimmune diseases.

Tumor metabolic reprogramming, particularly the Warburg effect, is one of the critical characteristics of tumor cells [29–31]. PTDSS1 may be a key molecule regulating this metabolic feature. The present study revealed that nuclear PTDSS1 plays a more crucial role in promoting lung cancer progression through glycolysis, providing a new perspective on the classical understanding of PTDSS1 function. Traditional views hold that PTDSS1 is primarily localized to the endoplasmic reticulum membrane and participates in membrane phospholipid synthesis, whereas the present study indicated that its nuclear localization may possess novel functions related to transcriptional regulation. These findings suggest a potential functional relationship between PTDSS1 and PKM2 in lung cancer progression, though the precise mechanistic basis of this interaction requires further investigation. While PKM2 silencing attenuated PTDSS1-mediated oncogenic effects, it could reflect general glycolytic inhibition rather than PKM2-specific mechanisms. The observed correlation between PTDSS1 and PKM2 expression in patient tissues and TCGA datasets, combined with co-localization studies demonstrating spatial proximity, supports potential molecular interaction. However, a definitive proof of direct binding and determination of regulatory directionality awaits future Co-immunoprecipitation (Co-IP) or Glutathione S-transferase (GST) pull-down experiments. Importantly, the relationship between PTDSS1 and PKM2 may be more complex than simple unidirectional regulation. Given PKM2's role as an allosteric target of serine and PTDSS1's involvement in serine-dependent phospholipid synthesis, both proteins may be co-regulated by metabolic factors rather than exhibiting direct regulatory control. Furthermore, the possibility of reverse regulation, where PKM2 influences PTDSS1 activity, cannot be excluded on the basis of current evidence. These mechanistic uncertainties highlight the correlative rather than causative nature of the present findings and underscore the need for comprehensive functional studies to establish definitive molecular relationships.

Another significant finding of this study is that PTDSS1 maintains mitochondrial homeostasis, inhibiting oxidative phosphorylation and apoptosis in lung cancer cells [24]. As the center of cellular energy metabolism and apoptotic regulation, mitochondrial dysfunction is closely associated with the development of various tumors [32,33]. Tumor cells typically maintain sufficient mitochondrial function and relatively low levels of oxidative phosphorylation, allowing them to adjust their metabolic patterns according to microenvironmental changes [34–36]. By maintaining mitochondrial homeostasis, PTDSS1 may provide tumor cells with this metabolic plasticity, conferring survival advantages in different microenvironments. PTDSS1 overexpression is predicted to significantly alter cellular phospholipid composition by increasing PtdSer synthesis from PtdEtn and PtdCho substrates. Such compositional changes could profoundly impact membrane biophysical properties, including fluidity, curvature, and protein–lipid interactions, with particular importance for mitochondrial function where precise lipid composition is essential for optimal respiratory chain activity. The observed reduction in OCR following PTDSS1 overexpression may result from altered mitochondrial membrane composition that impairs respiratory chain efficiency rather than, or in addition to, metabolic reprogramming toward glycolysis. The compensatory upregulation of PGC1-α, MFN1, and MFN2 observed in this study could represent cellular adaptation to mitochondrial dysfunction, attempting to restore mitochondrial mass and network connectivity despite reduced per-mitochondrion respiratory capacity. The 2-DG experiments provide preliminary evidence for glycolytic pathway involvement in PTDSS1-mediated chemoresistance, though these findings must be interpreted with caution. The absence of OE-NC cells treated with 2-DG represents an important experimental limitation because 2-DG's broad cytotoxic effects may confound the interpretation of its interaction with PTDSS1-mediated pathways. Future studies should include comprehensive dose–response analyses with appropriate controls to establish the specificity of metabolic pathway involvement in PTDSS1's protective functions.

Recent studies have found that PTDSS1 plays important roles in numerous tumors. Research has shown that inhibiting PTDSS1 expression can suppress lymphoma growth [8]. PS exposed on the cell surface has been targeted by the monoclonal antibody bavituximab in multiple ongoing clinical trials [37]. Studies have demonstrated that targeting PS in breast cancer can significantly inhibit tumor growth [38], indicating that while targeting PTDSS1's end product PS can inhibit tumor growth, PTDSS1 itself may also have potential as a therapeutic target. Therefore, identifying the role of targeting the PS-synthesizing enzyme PTDSS1 may have potential significance for tumor therapy. The finding that nuclear-targeted PTDSS1 exhibits en-

hanced oncogenic activity compared with native PTDSS1 distribution raises fundamental questions about the mechanistic basis of this compartment-specific function. This enhanced effect could result from several non-mutually exclusive mechanisms: (1) local nuclear PtdSer synthesis that modulates nuclear membrane composition, chromatin organization, or lipid-dependent nuclear signaling pathways; (2) catalytic activity-independent functions, where PTDSS1 serves as a scaffolding protein or direct regulator of nuclear transcriptional machinery; or (3) influence on nuclear-cytoplasmic metabolite gradients that affect gene expression programs. The distinction between these mechanisms has profound implications for understanding PTDSS1's role in cancer biology. Currently demonstrated in A549 cells only, this nuclear compartmentalization phenotype requires validation across multiple lung cancer cell lines to establish generalizability. The mechanistic basis of enhanced nuclear PTDSS1 activity represents one of the most important unresolved questions from this study and a high-priority direction for future investigation.

This study has several important limitations that must be acknowledged. The findings primarily demonstrated correlations rather than definitive causal relationships between PTDSS1 and PKM2 because the precise molecular mechanism underlying their interaction remains unclear, and the observed effects could reflect direct regulatory interactions or indirect consequences of altered cellular metabolism given PKM2's multifaceted regulatory roles. Additionally, the experimental design has notable gaps, including lack of direct evidence for physical PTDSS1-PKM2 interaction, uncertainty whether effects depend on PTDSS1's enzymatic activity or represent moonlighting functions, and 2-DG experiments lacking proper controls in non-overexpressing cells that may confound interpretation of glycolysis-specific versus general cytotoxic effects. Furthermore, expected phospholipid class distribution changes following PTDSS1 overexpression were not examined, and these changes could impact membrane composition and mitochondrial function through biophysical rather than transcriptional mechanisms. The reliance on cell line models may not fully recapitulate tumor heterogeneity and microenvironmental complexity despite including xenograft experiments and patient tissue correlation studies. The subcellular localization findings may be confounded by PTDSS1's known ER localization, particularly at mitochondrion-associated membranes, without appropriate ER marker controls. Future investigations should prioritize direct protein interaction studies, enzymatic versus non-enzymatic function assessment, comprehensive phospholipid profiling, and bidirectional functional studies to establish causal rather than associative relationships.

5. Conclusion

This study establishes PTDSS1 as a critical oncogenic driver in lung cancer through a previously uncharacterized dual regulatory mechanism. PTDSS1 overexpression correlates with poor clinical outcomes and drives malignant progression by orchestrating metabolic reprogramming via PKM2-mediated glycolytic enhancement while simultaneously maintaining mitochondrial homeostasis through upregulation of PGC-1α and MFN1/MFN2. Nuclear-localized PTDSS1 exhibits superior oncogenic efficacy, revealing a novel subcellular compartment-specific function beyond its classical endoplasmic reticulum role. This nuclear-mitochondrial crosstalk represents a sophisticated metabolic regulatory network that confers tumor cells enhanced proliferative capacity and apoptosis resistance. The identification of the PTDSS1-PKM2 axis provides a promising target for metabolic intervention in lung cancer, offering potential for selective disruption of tumor metabolism while preserving normal cellular function. These findings advance the understanding of metabolic reprogramming mechanisms and establish a foundation for developing precision therapeutic strategies targeting lung cancer metabolism.

Availability of Data and Materials

The datasets used and analyzed during the current study are available from the corresponding author on reasonable request.

Author Contributions

YL: Investigation, Data curation. HW: Formal analysis, Data curation. QW: Data curation. YH: Data curation. XP: Data curation. YL: Validation, Project administration. HW: Writing – original draft, Project administration. YL: Writing – review & editing. All authors contributed to editorial changes in the manuscript. All authors read and approved the final manuscript. All authors have participated sufficiently in the work and agreed to be accountable for all aspects of the work.

Ethics Approval and Consent to Participate

Human clinical samples: This study involving human participants was conducted in accordance with the Declaration of Helsinki. This study was approved by the hospital Ethics Committee of The Eighth Affiliated Hospital, Southern Medical University (The First People's Hospital of Shunde Foshan) (Approval No. 20250106-116). All patients voluntarily participated in the study and signed informed consent forms. Animal experiments: All animal experiments were conducted in accordance with the National Guidelines for Welfare and Ethics of Experimental Animals and the Guidelines for the Humane Treatment of Experimental Animals of China. The animal experiments met the ethical requirements and were approved by the Ethics Committee of The Third Affiliated Hospital of Zunyi Medical University (Approval No. (2023)-2-295).

Acknowledgment

Not applicable.

Funding

This work was supported by the Natural Science Foundation of Guizhou Province (Grant No. ZK[2023]486).

Conflict of Interest

The authors declare no conflict of interest.

Supplementary Material

Supplementary material associated with this article can be found, in the online version, at https://doi.org/10.31083/FBL45020.

References

[1] Faubert B, Solmonson A, DeBerardinis RJ. Metabolic reprogramming and cancer progression. Science (New York, N.Y.). 2020; 368: eaaw5473. https://doi.org/10.1126/science.aaw5473.

[2] Xu X, Peng Q, Jiang X, Tan S, Yang Y, Yang W, *et al*. Metabolic reprogramming and epigenetic modifications in cancer: from the impacts and mechanisms to the treatment potential. Experimental & Molecular Medicine. 2023; 55: 1357–1370. https://doi.org/10.1038/s12276-023-01020-1.

[3] Bose S, Zhang C, Le A. Glucose Metabolism in Cancer: The Warburg Effect and Beyond. Advances in Experimental Medicine and Biology. 2021; 1311: 3–15. https://doi.org/10.1007/978-3-030-65768-0_1.

[4] Fukushi A, Kim HD, Chang YC, Kim CH. Revisited Metabolic Control and Reprogramming Cancers by Means of the Warburg Effect in Tumor Cells. International Journal of Molecular Sciences. 2022; 23: 10037. https://doi.org/10.3390/ijms231710037.

[5] Vaupel P, Multhoff G. Revisiting the Warburg effect: historical dogma versus current understanding. The Journal of Physiology. 2021; 599: 1745–1757. https://doi.org/10.1113/JP278810.

[6] Fan M, Shi Y, Zhao J, Li L. Cancer stem cell fate determination: mito-nuclear communication. Cell Communication and Signaling: CCS. 2023; 21: 159. https://doi.org/10.1186/s12964-023-01160-x.

[7] He B, Gao R, Lv S, Chen A, Huang J, Wang L, *et al*. Cancer cell employs a microenvironmental neural signal trans-activating nucleus-mitochondria coordination to acquire stemness. Signal Transduction and Targeted Therapy. 2023; 8: 275. https://doi.org/10.1038/s41392-023-01487-4.

[8] Yoshihama Y, Namiki H, Kato T, Shimazaki N, Takaishi S, Kadoshima-Yamaoka K, *et al*. Potent and Selective PTDSS1 Inhibitors Induce Collateral Lethality in Cancers with PTDSS2 Deletion. Cancer Research. 2022; 82: 4031–4043. https://doi.org/10.1158/0008-5472.CAN-22-1006.

[9] Sousa SB, Jenkins D, Chanudet E, Tasseva G, Ishida M, Anderson G, *et al*. Gain-of-function mutations in the phosphatidylserine synthase 1 (PTDSS1) gene cause Lenz-Majewski syndrome. Nature Genetics. 2014; 46: 70–76. https://doi.org/10.1038/ng.2829.

[10] Sekar D, Dillmann C, Sirait-Fischer E, Fink AF, Zivkovic A, Baum N, *et al*. Phosphatidylserine Synthase PTDSS1 Shapes the Tumor Lipidome to Maintain Tumor-Promoting Inflammation. Cancer Research. 2022; 82: 1617–1632. https://doi.org/10.1158/0008-5472.CAN-20-3870.

[11] Lei Y, Zhou B, Meng X, Liang M, Song W, Liang Y, *et al*. A risk score model based on lipid metabolism-related genes could predict response to immunotherapy and prognosis of lung adenocarcinoma: a multi-dataset study and cytological validation. Discover Oncology. 2023; 14: 188. https://doi.org/10.1007/s12672-023-00802-3.

[12] Schiliro C, Firestein BL. Mechanisms of metabolic reprogramming in cancer cells supporting enhanced growth and proliferation. Cells. 2021; 10: 1056. https://doi.org/10.3390/cells10051056.

[13] Shuvalov O, Daks A, Fedorova O, Petukhov A, Barlev N. Linking Metabolic Reprogramming, Plasticity and Tumor Progression. Cancers. 2021; 13: 762. https://doi.org/10.3390/cancers13040762.

[14] Zhao H, Ji Y, Liang C. Solute carrier family 6 member 3 promotes the development of clear cell renal cell carcinoma by enhancing glycolysis and inhibiting ferroptosis. CytoJournal. 2025; 22.

[15] Zahra K, Dey T, Ashish, Mishra SP, Pandey U. Pyruvate Kinase M2 and Cancer: The Role of PKM2 in Promoting Tumorigenesis. Frontiers in Oncology. 2020; 10: 159. https://doi.org/10.3389/fonc.2020.00159.

[16] Gupta V, Iqbal MA, Kumar B, Bamezai RN. Pyruvate kinase M2: a metabolic tuner. In Tumor Cell Metabolism: Pathways, Regulation and Biology (pp. 123–142). Springer: Vienna. 2015.

[17] Todisco S, Iacobazzi D, Santarsiero A, Convertini P, Infantino V. Nuclear functional role of metabolic enzymes and related metabolites: Focus on gene expression regulation. Molecular Metabolism. 2025; 100: 102233. https://doi.org/10.1016/j.molmet.2025.102233.

[18] Zhao H, Jiang R, Feng Z, Wang X, Zhang C. Transcription factor LHX9 (LIM Homeobox 9) enhances pyruvate kinase PKM2 activity to induce glycolytic metabolic reprogramming in cancer stem cells, promoting gastric cancer progression. Journal of Translational Medicine. 2023; 21: 833. https://doi.org/10.1186/s12967-023-04658-7.

[19] Lopez J, Tait SWG. Mitochondrial apoptosis: killing cancer using the enemy within. British Journal of Cancer. 2015; 112: 957–962. https://doi.org/10.1038/bjc.2015.85.

[20] Vyas S, Zaganjor E, Haigis MC. Mitochondria and Cancer. Cell. 2016; 166: 555–566. https://doi.org/10.1016/j.cell.2016.07.002.

[21] Jin P, Jiang J, Zhou L, Huang Z, Nice EC, Huang C, *et al*. Mitochondrial adaptation in cancer drug resistance: prevalence, mechanisms, and management. Journal of Hematology & Oncology. 2022; 15: 97. https://doi.org/10.1186/s13045-022-01313-4.

[22] Wei H, Qu L, Dai S, Li Y, Wang H, Feng Y, *et al*. Structural insight into the molecular mechanism of p53-mediated mitochondrial apoptosis. Nature Communications. 2021; 12: 2280. https://doi.org/10.1038/s41467-021-22655-6.

[23] Michalek S, Brunner T. Nuclear-mitochondrial crosstalk: On the role of the nuclear receptor liver receptor homolog-1 (NR5A2) in the regulation of mitochondrial metabolism, cell survival, and cancer. IUBMB Life. 2021; 73: 592–610. https://doi.org/10.1002/iub.2386.

[24] Liu L, Li Y, Chen G, Chen Q. Crosstalk between mitochondrial biogenesis and mitophagy to maintain mitochondrial homeostasis. Journal of Biomedical Science. 2023; 30: 86. https://doi.org/10.1186/s12929-023-00975-7.

[25] Fan M, Shi Y, Zhao J, Li L. Cancer stem cell fate determination: mito-nuclear communication. Cell Communication and Signaling. 2023; 21: 159. https://doi.org/10.1186/s12964-023-01160-x.

[26] Soueid J, Kourtian S, Makhoul NJ, Makoukji J, Haddad S, Ghanem SS, *et al*. RYR2, PTDSS1 and AREG genes are implicated in a Lebanese population-based study of copy num-

ber variation in autism. Scientific Reports. 2016; 6: 19088. https://doi.org/10.1038/srep19088.

[27] Suzuki K, Itoh R, Oyama J, Hayashi M, Ueda T. Efficient Multikilogram-Scale Synthesis of PTDSS1 Inhibitor: Development of a Practical and Scalable Optical Resolution Method for Chiral 2, 3-Pyrrolidinedione. Organic Process Research & Development. 2024; 28: 2296–2308. https://doi.org/10.1021/acs.oprd.4c00056.

[28] Kur IM, Weigert A. Phosphatidylserine externalization as immune checkpoint in cancer. Pflugers Archiv: European Journal of Physiology. 2024; 476: 1789–1802. https://doi.org/10.1007/s00424-024-02948-7.

[29] Li AM, Ye J. Deciphering the Warburg effect: metabolic reprogramming, epigenetic remodeling, and cell dedifferentiation. Annual Review of Cancer Biology. 2024; 8: 35–58. https://doi.org/10.1146/annurev-cancerbio-062822-120857.

[30] Li Z, Sun C, Qin Z. Metabolic reprogramming of cancer-associated fibroblasts and its effect on cancer cell reprogramming. Theranostics. 2021; 11: 8322–8336. https://doi.org/10.7150/thno.62378.

[31] Yang F, Hilakivi-Clarke L, Shaha A, Wang Y, Wang X, Deng Y, *et al*. Metabolic reprogramming and its clinical implication for liver cancer. Hepatology (Baltimore, Md.). 2023; 78: 1602–1624. https://doi.org/10.1097/HEP.0000000000000005.

[32] Palikaras K, Lionaki E, Tavernarakis N. Balancing mitochondrial biogenesis and mitophagy to maintain energy metabolism homeostasis. Cell Death and Differentiation. 2015; 22: 1399–1401. https://doi.org/10.1038/cdd.2015.86.

[33] Bathina S, Das UN. Role of Mitochondrial Dysfunction in Cellular Lipid Homeostasis and Disease. Discovery Medicine. 2023; 35: 653–663. https://doi.org/10.24976/Discov.Med.202335178.64.

[34] Li W, Kui L, Demetrios T, Gong X, Tang M. A Glimmer of Hope: Maintain Mitochondrial Homeostasis to Mitigate Alzheimer's Disease. Aging and Disease. 2020; 11: 1260–1275. https://doi.org/10.14336/AD.2020.0105.

[35] Fu J, Hu F, Ma T, Zhao WJ, Tian H, Zhang Y, *et al*. A conventional immune regulator mitochondrial antiviral signaling protein blocks hepatic steatosis by maintaining mitochondrial homeostasis. Hepatology (Baltimore, Md.). 2022; 75: 403–418. https://doi.org/10.1002/hep.32126.

[36] Wu J, Subbaiah KCV, Hedaya O, Chen S, Munger J, Tang WHW, *et al*. FAM210A regulates mitochondrial translation and maintains cardiac mitochondrial homeostasis. Cardiovascular Research. 2023; 119: 2441–2457. https://doi.org/10.1093/cvr/cvad124.

[37] Chalasani P, Marron M, Roe D, Clarke K, Iannone M, Livingston RB, *et al*. A phase I clinical trial of bavituximab and paclitaxel in patients with HER2 negative metastatic breast cancer. Cancer Medicine. 2015; 4: 1051–1059. https://doi.org/10.1002/cam4.447.

[38] Gray MJ, Gong J, Hatch MMS, Nguyen V, Hughes CCW, Hutchins JT, *et al*. Phosphatidylserine-targeting antibodies augment the anti-tumorigenic activity of anti-PD-1 therapy by enhancing immune activation and downregulating pro-oncogenic factors induced by T-cell checkpoint inhibition in murine triple-negative breast cancers. Breast Cancer Research: BCR. 2016; 18: 50. https://doi.org/10.1186/s13058-016-0708-2.